Articles in PresS. Am J Physiol Heart Circ Physiol (September 16, 2016). doi:10.1152/ajpheart.00156.2016

Changes in cardiac $Na_V1.5$ expression, function, and acetylation by pan-histone deacetylase inhibitors

Qin Xu[1#], Dakshesh Patel[1#], Xian Zhang[1#], and Richard D Veenstra[1,2]

[1]Department of Pharmacology, SUNY Upstate Medical University, Syracuse, NY 13210

[2]Dept. of Cell and Molecular Biology, SUNY Upstate Medical University, Syracuse, NY 13210

#These authors contributed equally to the manuscript and should be considered co-first authors

Author Contributions

Qin Xu performed the TSA and VOR I_{Na} and $Na_V1.5$ experiments and FK228 g_j measurements.

Dakshesh Patel performed the FK228 I_{Na}, PCR, HDAC activity assay, and hiPSC-CM experiments.

Xian Zhang performed the new hiPSC-CM I_{Na} experiments and $Na_V1.5$ immunoprecipitation:immunoblot experiments.

Richard D Veenstra planned and directed the project, analyzed the I_{Na} inactivation kinetics, performed the bioinformatics analyses of the $Na_V1.5$ sequences, and wrote the manuscript with input from the co-authors.

Running Title: Changes in cardiac I_{Na} by pan-HDAC inhibition

Address for Correspondence:

Richard D Veenstra, Ph.D., Department of Pharmacology, SUNY Upstate Medical University, 750 East Adams Street, Syracuse, NY 13210; Phone: 315-464-5145; Fax: 315-464-8014; E-mail: veenstrr@upstate.edu

Abstract

Histone deacetylase (HDAC) inhibitors are small molecule anti-cancer therapeutics that exhibit limiting cardiotoxicities including QT interval prolongation and life-threatening cardiac arrhythmias. Because the molecular mechanisms for HDAC inhibitor-induced cardiotoxicity are poorly understood, we performed whole cell patch voltage clamp experiments to measure cardiac sodium currents (I_{Na}) from wild-type neonatal mouse ventricular or human induced pluripotent stem cell derived cardiomyocytes treated with trichostatin A (TSA), vorinostat (VOR), or romidepsin (FK228). All three pan-HDAC inhibitors dose-dependently decreased peak I_{Na} density and shifted the voltage activation curve 3-8 mV positive. Increases in late I_{Na} were not observed despite a moderate slowing of the inactivation rate at low activating potentials (<40 mV). *Scn5a* mRNA levels were not significantly altered but $Na_V1.5$ protein levels were significantly reduced. Immunoprecipitation with anti-$Na_V1.5$ and Western blotting with anti-acetyl-lysine antibodies indicated that $Na_V1.5$ acetylation is increased *in vivo* after HDAC inhibition. FK228 inhibited total cardiac HDAC activity with two apparent IC_{50}s of 5 nM and 1.75 μM, consistent with previous findings with TSA and VOR. FK228 also decreased ventricular gap junction conductance (g_j), again consistent with previous findings. We conclude that pan-HDAC inhibition reduces cardiac I_{Na} density and $Na_V1.5$ protein levels without affecting late I_{Na} amplitude and, thus, probably doesn't contribute to the reported QT interval prolongation and arrhythmias associated with pan-HDAC inhibitor therapies. Conversely, reductions in g_j may enhance the occurrence of triggered activity by limiting electrotonic inhibition and, combined with reduced I_{Na}, slow myocardial conduction and increase vulnerability to reentrant arrhythmias.

48

49 **New and Noteworthy**

50 Therapeutic histone deacetylase inhibition with vorinostat or romidepsin significantly reduces
51 ventricular sodium current density and $Na_V1.5$ protein expression. A slight positive shift in the
52 voltage activation curve, presumably the result of lysine acetylation, decreases the inactivation
53 rate at low activating potentials but does not increase the late sodium current amplitude.

54

55 **Keywords:** trichostatin A, vorinostat, romidepsin, sodium current, gap junctions

Introduction

Histone deacetylase (HDAC) inhibitors represent a novel class of small molecule therapeutics with indications for the treatment of numerous human disorders including cancer, neurodegenerative diseases, type 2 diabetes, and autoimmunity (20, 22, 24, 28, 58). HDAC inhibitors are divided into four major chemical subgroups, the hydroxamic acid derivatives, benzamides, cyclic peptides, and short chain fatty acids (50). The naturally-occurring prototypical hydroxamic acid and cyclic peptide HDAC inhibitors, trichostatin A (TSA) and romidepsin (depsipeptide, FK228), inhibit all eleven Zn^{2+}-dependent human HDAC isoforms (1-11) with high (nM-μM) affinity and are considered to be pan-HDAC inhibitors (5). In contrast, the benzamide derivatives like entinostat (MS-275) and mocetinostat (MGCD-0103) are high affinity inhibitors of only the class I HDACs (HDAC1, 2, 3 and 8). Class IIb inhibitors target HDAC6 with relative specificity and Class IIa (HDACs 4, 5, 7, and 9) are under development (11, 34). Four pan-HDAC inhibitors have received Food and Drug Administration (FDA) approval since 2006, all for the treatment of cutaneous and/or peripheral T cell lymphoma (CTCL and/or PTCL) or multiple myeloma (MM) (14). Cardiac arrhythmias have been associated with the clinical use of HDAC inhibitors since 2006 and the reported global incidence of HDAC inhibitor-induced adverse cardiac side effects is 28.6% (17, 50, 55, 57). Two of the FDA approved HDAC inhibitors, romidepsin (Istodax®) and panobinostat (LBH589, Farydak®) carry warnings for severe ECG changes and cardiac arrhythmias including ventricular tachycardias, although grade 3 or higher QT interval prolongations and ventricular fibrillation have occasionally occurred with vorinostat (SAHA, VOR, Zolinza®) and belinostat (PXD101, Beleodaq®) (14, 15, 36).

We previously reported that TSA and VOR dose-dependently decreased connexin43 (Cx43) expression and electrical coupling between ventricular cardiomyocytes (71). The Duchenne muscular dystrophic (mdx) mouse model exhibits a hyperacetylated protein state resulting in acetylated Cx43, a decrease in $Na_V1.5$ cardiac sodium channel protein expression, and an increased incidence of restraint-induced cardiac arrhythmias (8, 9). The N^{ε}-lysine acetylated Cx43 dissociates from ventricular gap junctions, which may account for the stress-induced increased arrhythmogenesis in mdx mice (9). Treatment of mdx mice with VOR reduced the incidence of stress-induced arrhythmias and improved Cx43 localization to the intercalated disc. Conversely, mdx mice exhibited a lower incidence of arrhythmias than wild-type mice when treated with aconitine, a sodium channel opener, and VOR administration increased the incidence of these arrhythmias in mdx mice, suggesting functional differences in the cardiac sodium current between control and mdx mice (8). Since loss of Cx43 myocardial gap junctions is associated with reductions in cardiac sodium current (I_{Na}) carried by the $Na_V1.5$ channel protein, we chose to study the effect of pan-HDAC inhibition on cardiac I_{Na} (25, 46). In this study we report our findings of TSA, VOR, and FK228 effects on the cardiac sodium current (I_{Na}). This is the first reported study to examine the effects of pan-HDAC inhibition on cardiac I_{Na} in wild-type cardiomyocytes and these three HDAC inhibitors all decreased I_{Na} density in a dose-dependent manner. Additionally, a slight 3 - 8 mV positive shift in the steady-state voltage-dependent activation curve was observed with high doses of TSA and VOR without a concomitant shift in the inactivation curve. No increases in late I_{Na} were observed, suggesting that the only contribution of pan-HDAC inhibition to I_{Na}-dependent cardiac arrhythmias may be attributed to decreased excitability and slowed conduction, especially when combined with decreased myocardial gap junction coupling.

Materials and Methods

Cell culture

Newborn C57BL/6 mice were anesthetized with isoflurane and the hearts excised in accordance with the recommendations in the Guide for the Care and Use of Laboratory Animals of the National Institutes of Health. The protocol (IACUC #263) was approved by the Institutional Animal Care and Use Committee (IACUC) of SUNY Upstate Medical University. The atria and ventricles were dissociated separately and cultured in Medium 199 (M199) supplemented with 10% FBS as previously described (71). Neonatal mouse ventricular myocytes (NMVMs) were cultured at low ($\approx 2 \times 10^{+5}$ cells/35 mm culture dish) or high ($\approx 10^{+7}$ cells/35 mm culture dish) density for patch clamp and real-time PCR (RT-PCR) or Western blot procedures, respectively. Cryopreserved human induced-pluripotent stem cell-derived cardiomyocytes (hiPSC-CM, iCell cardiomyocytes) were purchased from Cellular Dynamics Inc. (CDI, Madison, WI) and plated and grown in culture media and prepared for electrophysiological experiments per manufacturer's instructions (37).

HDAC Inhibitors

Trichostatin A (TSA) was purchased from Calbiochem or ENZO Life Sciences and 1 mg was dissolved in DMSO and stored at -20 °C. Vorinostat (VOR) and romidepsin (FK228) were purchased from Selleck Chemicals, dissolved in DMSO, and stored at -20 °C. The 100 mM DMSO stock solutions of TSA, VOR, and FK228 were diluted to the desired experimental test concentrations in M199 or maintenance media and applied to NMVM or hiPSC-CM cultures overnight for 18-24 hrs prior to experimental procedures. Final DMSO levels were < 0.005% (v/v).

Whole cell patch clamping

Single whole cell patch electrode voltage clamp experiments were performed on NMVMs and hiPSC-CMs using conventional procedures with an Alembic Instruments Ve-2, Axopatch 1D, or Axopatch 200B patch clamp amplifier, Digidata 1320A or 1440 A/D converter, and pClamp8.2 or 10.1 software (Molecular Devices). Voltage-gated sodium currents (I_{Na}) were elicited from a holding potential (V_h) of -120 mV during voltage steps from -90 mV to +50 mV in 5 mV increments for 150 ms using reduced NaCl solutions (Table 1). For the I_{Na} inactivation protocol, V_h was -120 mV and the prepulse voltage increased from -130 mV to -30 mV in +5 mV increments for 150 ms followed by a 30 ms activation step to -40 mV. In some experiments, 30 μM TTX was added to the bath to verify that the inward current was TTX-sensitive. Gap junction conductance (g_j) measurements were obtained using conventional dual whole cell patch clamp procedures as previously described (64, 71).

Table 1. Electrophysiological Solutions

Composition (mM)	Normal Saline	Pipette Solution	Low Na^+ Saline	I_{Na} pipette Solution	hiPSC-CM Saline	CM pipette Solution
NaCl	140	---	20	5	30	5
KCl	1.3	140	---	---	---	---
TMACl[1]	---	---	100	115	---	---
TEACl[2]	---	---	20	20	110	135
CsCl	---	---	---	---	5	5
NaH_2PO_4	1.0	---	---	---	---	---
$CaCl_2$	1.8	3.0	1.8	3.0	1.8	3.0
$MgCl_2$/($MgSO_4$)	(0.8)	1.0	1.0	1.0	1.0	1.0
Glucose	5.5	---	5.5	---	5.5	---
$BaCl_2$ & $CdCl_2$	---	---	0.1 & 0.1	---	---	---
BAPTA/(EGTA)	---	5.0	---	5.0	---	(5)
HEPES*	10	25	10	20	20	20

[1]tetramethylammoniumCl (TMACl); [2]tetramethylammoniumCl (TEACl)

*pH was titrated to 7.4 with 1N NaOH, KOH, TEAOH, or CsOH..

Real-time PCR

Cellular RNA was extracted from cultured NMVMs and 10 µl RT-PCR reactions were carried out on 384 well plates using *LightCycler*® 480 Real-Time PCR System (Roche) using previously published procedures (71). All results were normalized to *Gapdh* and control samples. cT values were determined by the apparatus and the quality of the PCR product was confirmed by analyzing the melt-curve. Since HDAC inhibition is known to alter housekeeping gene expression (45), the control and VOR *Gapdh* cT and relative (to control) expression level values were analyzed statistically and found to not be significantly different (paired t-test, $p > 0.25$). Primer sets for murine *Cdh2*, *Gja1, Scn5a*, *and Slc8a*, *Cdh2*, and were designed to span exon-intron regions of the gene of interest. The murine forward and reverse primer sequences are: *Cdh2,* 5'-TATGTGATGACGGTCACTGC-3' and 5'-GAAAGGCCAT AAGTGGGATT-3'; *Gapdh,* 5'- TGCCACTCAGAAGACTGTGG-3' and 5'-AGGAATGGGAGTTGCTGTTG-3'; *Gja1,* 5'-GAGAGCCCGAACTCTCCTTT-3' and 5'-TGGAGTAGGCTTGGACCTTG-3'; *Scn5a,* 5'-CTTCACCAACAGCTGGAACA-3' and 5'-GACATCATGAGGGCGAAGAG-3'; and *Slc8a,* 5'-TGAATCTTGCACGCTCATTA-3' and 5'-CCAGGCACATCCAAAGTATC-3'.

Western blotting

NMVMs were cultured for 3 days in 200 µM bromodeoxyuridine (BrDU)/M199 media supplemented with 10% fetal FBS and 10/10 U/µg penicillin/streptomycin. TSA, VOR, or 3 ml of control BrDU/M199 media was added overnight. On the fourth day, the NMVM cultures were harvested, lysed, and 15 µg protein samples underwent immunoblot procedures as previously

described using ECL™ Western Blot Detection Reagents (Bio-Rad Labs, Hercules, CA; 71). The rabbit polyclonal anti-$Na_V1.5$ (Cat. #ASC-005) primary antibody was purchased from Alomone Labs (Jerusalem, Israel), the mouse monoclonal anti-α-tubulin antibody (Cat. # T8203, clone AA13) was purchased from Sigma-Aldrich (St. Louis, MO), and the rabbit polyclonal anti-acetylated-α-tubulin and HDAC1 (Cat. #BML-SA452 and BML-SA401) antibodies were purchased from Enzo Life Sciences (Farmingdale, NY).

Immunoprecipitation

Six adult C57BL/6 mice were i.p. injected with either 10 mg/kg TSA (1 mg/ml in sterile saline:5% DMSO, n=3) or saline:DMSO (10 µl/gm body weight, n=3) daily for five consecutive days and sacrificed 4-6 hours after the last injection as approved by the SUNY Upstate Medical University IACUC. The hearts were excised under ketamine/xylazine anesthesia, atria and ventricles were separated, and lysed in 1% Triton X-100 extraction buffer (50 mM Tris, pH 8.0, 150 mM NaCl, 0.02% sodium azide, 1.0 mM PMSF, 1 µg Aprotinin, 1% Triton X-100, 1 mM Na_3VO_4, 50 mM NaF) with protease inhibitors (Roche). The ventricular heart lysates were subjected to immunoprecipitation (IP) and Western blot procedures using primary anti-$Na_V1.5$ and anti-acetyl-lysine (Ac-K, Abcam, Cat. # ab21623) rabbit polyclonal antibodies and the Dynabeads® Protein G (ThermoFisher Scientific) immunoprecipitation procedures. The primary antibody was bound to the Protein G magnetic beads according to manufacturer's instructions and the target antigen ($Na_V1.5$) was immunoprecipitated in an IP buffer containing 1% Triton X-100, 0.5% NP-40, 20 mM HEPES, 50 mM NaCl, and protease inhibitors (Roche), pH 7.4, using a magnet. The immunoprecipitate was washed with washing buffer, eluted with elution buffer, subjected to SDS-PAGE electrophoresis and Western blot procedures with anti-Ac-K and anti-

186 $Na_V1.5$ antibodies as previously described. The $Na_V1.5$ immunoprecipitation experiments were
187 performed in triplicate.
188
189 ***HDAC activity assay***
190 Aliquots of 6 x 10^{+5} NMVMs per well (96-well plate) were grown in 200 µl of 200 µM
191 bromodeoxyuridine (BrDU)/M199, exchanged daily. Cell wells were incubated with 2,000
192 pmoles of the acetylated Fluor-de-Lys® substrate for 6 hours during continuous (overnight)
193 HDAC inhibition (71). Cell, media, and standard curve deacetylated substrate sample wells were
194 developed according to manufacturer's directions (BML-AK503 HDAC fluorometric cellular
195 activity assay kit (Enzo Life Sciences) and background subtracted relative fluorescence unit
196 (RFU) counts were acquired with a BIO-TEK Synergy H1 plate reader (360 nm excitation, 460
197 nm emission).
198
199 ***Statistics***
200 Averaged values are presented as the Mean ± SEM. Statistical analyses were performed with the
201 Normality and one-way ANOVA tests using the Bonferroni method in Origin 8.6. Statistical
202 comparisons of the late (100 ms) I_{Na} datasets was performed using the F-test comparison of Two
203 Datasets function in Origin7.5.
204
205

Results

Effects of pan-HDAC inhibition on cardiac Na^+ current density

To examine the effect of pan-HDAC inhibition on functional cardiac I_{Na}, cultured NMVMs were incubated overnight with 50 or 100 nM TSA, 1 or 5 μM VOR, or 10 nM FK228 and whole cell patch clamp experiments were performed the next day (18-24 hrs later). To activate I_{Na}, NMVM membrane potential (V_m) was depolarized between -90 and +60 mV in 150 ms, 5 mV increments from a V_h of -120 mV. Examples of I_{Na} current traces elicited from control, 100 nM TSA, 1 μM VOR, and 10 nM FK228 treated NMVMs are illustrated in Figures 1A-D. Peak I_{Na} density decreased from control values of -36.2 ± 2.8 pA/pF to -13.7 ± 2.5 pA/pF with 100 nM TSA, -17.6 ± 1.7 pA/pF with 5 μM VOR, and -15.1 ± 2.0 pA/pF with 10 nM FK228 (Figs. 1F-H). Cellular input capacitance values were not significantly changed from control values (22.5 ± 1.4 pF, n=20) except at the highest concentrations of TSA (100 nM; 15.3 ± 0.7 pF, n=17) and VOR (5 μM; 16.2 ± 0.7 pF, n=24) tested. The results are consistent with a pan-HDAC inhibitor-induced reduction in peak cardiac I_{Na} irrespective of whether the HDAC inhibitor belongs to the hydroxamate or cyclic peptide chemical group of HDAC inhibitors.

Persistent activation of I_{Na}, caused by mutations in the $Na_V1.5$ sodium channel protein that inhibit inactivation (e.g. ΔKPQ) or the α-sodium channel toxins like aconitine, are known to cause cardiac arrhythmias via induction of early afterdepolarizations (EADs) (8, 65). Thus, we measured the steady state current values at 100 ms for all control, 100 nM TSA, 1 μM VOR, and 10 nM FK228 experiments. Linear regression analyses of the whole cell current measured at the 100 ms time point of the voltage clamp steps from -120 mV to -65 through 0 mV for all four experimental groups revealed no significant differences in the slopes (+0.37, +0.24, +0.34, and

+0.44 pA/mV for Control, TSA, VOR, and FK228, respectively) of all four datasets. The y-intercepts were significantly ($p<0.05$) more negative (19 pA inward) for TSA and significantly more positive (6 pA outward) for FK228 relative to Control and VOR values. Taken together, there is no evidence of an increase in the late I_{Na} current in ventricular cardiomyocytes with either of the clinically approved HDAC inhibitors tested.

I_{Na} activation and inactivation

A slight positive shift in the activation voltage is apparent in the I_{Na} current-voltage relationships in Figs. 1F-H, so the peak sodium conductances (gNa) were calculated by dividing the normalized peak I_{Na} density values by ($V_m - E_{Na}$) for each I-V curve in Fig. 1 and normalized by dividing by the average maximum gNa ($\bar{g}$ Na) for each experimental group. The calculated Nernst potential for Na^+ (E_{Na}) was +35 mV and the experimental reversal potential (E_{rev}) values were within 5 mV or ±1 pA/pF of E_{Na} for all experimental groups. The V_m-dependent activation curves for TSA, VOR, and FK228 (Fig. 2A-C) illustrate a +3 to +8 mV shift in the half activation voltage ($V_{½act}$) for all three pan-HDAC inhibitor experimental groups. Since I_{Na} activation was slightly affected by the HDAC inhibitor treatments, I_{Na} inactivation was examined using a prepulse protocol illustrated in Fig. 2E. The highest inhibitory concentrations of TSA (100 nM) and VOR (5 μM) tested shifted the control I_{Na} half-inactivation voltage ($V_{½inact}$) of -83 mV by less than ±1 mV (Fig. 2D). The effect of FK228 on I_{Na} inactivation was not examined. The small positive shift in the I_{Na} activation curves without an accompanying change in the inactivation curve decreases the V_m-dependent "window" for persistent I_{Na} activation (Fig. 2F).

The time-dependence of I_{Na} inactivation was also examined by curve-fitting the decaying phase of the I_{Na} traces with a first-order exponential function. The V_m-dependent inactivation time constants (τ_h) were significantly slower in the -60 to -45 mV range for 100 nM TSA and 1 μM VOR, but not for 10 nM FK228 (Fig. 3A-C). There was no difference in the inactivation rates between control and HDAC inhibitor treated ventricular cardiomyocytes within the -40 to -10 mV range, suggesting that the slow τ_h values at low activating voltages seen with pan-HDAC inhibition result from the positive shift in the activation curves (Fig. 2A-C) and that I_{Na} inactivation rates were otherwise unaffected.

hiPSC cardiomyocytes

To assess whether the pan-HDAC inhibitor-induced decrease in cardiac I_{Na} occurs in human ventricular myocytes, human induced pluripotent stem cell derived cardiomyocytes (hiPSC-CMs) were treated with 1 μM VOR and I_{Na} whole cell patch clamp experiments were performed (Fig. 4). In hiPSC-CMs, the recommended human therapeutic dose of VOR reduced cardiac I_{Na} density by 52% relative to control experiments, indicating that NMVMs are a valid experimental model for studying the effects of HDAC inhibitors on cardiac I_{Na}. The mean whole cell current, measured between 100 and 150 ms, did not reveal any increase in late inward currents in the VOR hiPSC-CM group relative to the control group, consistent with our findings in NMVMs suggesting that late I_{Na} was not induced by clinically relevant HDAC inhibitor treatments.

$Na_V1.5$ expression

Experiments in NMVMs and hiPSC-CMs consistently indicate that pan-HDAC inhibition reduced I_{Na} density, but the molecular basis for the decrease in cardiac I_{Na} is unknown. The shift

in the I_{Na} activation curve is not sufficient to decrease peak I_{Na} levels and only slowed the inactivation kinetics at low activating potentials (<-40 mV). To test the hypothesis that pan-HDAC inhibition may be decreasing the $Na_V1.5$ protein expression level, real-time PCR and Western blot experiments were performed on NMVM cultures under control and pan-HDAC inhibitor treated conditions. The relative *Scn5a* mRNA abundance was less than that observed for *Gja1*, *Cdh2*, or *Slc8* and all were <50% of *Gapdh* levels (Fig. 5A). As previously reported, the *Gja1* and *Cdh2* mRNA levels were significantly reduced by 1 μM VOR (71), but *Scn5a* and *Slc8a* mRNA levels were not significantly different from control values (Fig. 5B). 100 nM TSA did reduce *Scn5a* mRNA levels by 50% (N = 2), but did not reach statistical significance (p> 0.05). However, Western blot analyses, performed in triplicate, revealed that $Na_V1.5$ protein levels were significantly reduced at all concentrations of TSA and VOR tested. The decrease in I_{Na} density correlates closely (within 15-25% deviation from unity) with the reduction in $Na_V1.5$ protein levels for both TSA and VOR, suggesting that the molecular basis for the pan-HDAC inhibitor induced decrease in cardiac I_{Na} is the dose-dependent reduction in $Na_V1.5$ protein expression. Real-time PCR results with10 nM FK228 exhibited qualitatively similar abundances for the *Chd2*, *Gja1*, *Scn5a*, and *Slc8a* genes and a significant reduction in their mRNA levels relative to control values for all except the Scn5a gene transcript levels (Fig. 5E).

Inhibition of cardiac HDAC activity by romidepsin

To correlate the decreases of cardiac I_{Na} and Cx43 mRNA expression levels with the HDAC inhibitory activity of FK228, the total NMVM HDAC activity was measured using a fluorimetric HDAC activity assay in the presence of increasing [FK228] to detect the amount of deacetylated Fluor-de-Lys® substrate using previously published procedures (71). As reported for TSA and

297 VOR, inhibition of total cardiac HDAC activity by FK228 exhibited two affinities with the
298 higher affinity site possessing at least twice the capacity of the lower affinity site (Fig. 6A). The
299 IC_{50} values for FK228 were 5.4 ± 0.6 nM and 1.75 ± 0.47 μM with capacities of 63.5% and
300 27.7% of total HDAC activity, respectively. Thus, 10 nM FK228 corresponds to twice the IC_{50}
301 of the high affinity HDAC inhibitory site and is far below the threshold concentration for the
302 secondary low affinity site previously associated with significant reductions in Cx43 expression
303 and function (71). Since TSA and VOR reduced cardiac g_j in a dose-dependent manner, we
304 assessed the dose-dependent effects of FK228 on initial g_j values of NMVM cell pairs (Fig. 6B).
305 Consistent with our previous findings, FK228 concentrations > 1 nM significantly decreased g_j.
306
307 **Discussion**
308 This study consistently found that pan-HDAC inhibition reduced peak I_{Na} density and $Na_V1.5$
309 protein levels (Figs. 1, 4, and 5). The only other functional alteration of cardiac I_{Na} observed with
310 pan-HDAC inhibition was a slight (3-8 mV) shift in the V_m-dependent activation curve and a
311 subsequent slowing of the inactivation time constants at low activating potentials (< -40 mV).
312 *Scn5a* mRNA levels were not decreased by 1 μM VOR yet there was a 40% reduction in $Na_V1.5$
313 protein levels (Fig. 5B-D). The 400 mg daily maximum recommended human therapeutic dose
314 of VOR correlates to a maximum plasma concentration (C_{max}) value of ≈ 1.2 μM (320 ng/ml)
315 (29). Reduced $Na_V1.5$ protein levels and I_{Na} density without a concomitant decrease in *Scn5a*
316 mRNA levels have also been reported in mdx mice (16). TTX-sensitive sodium channel isoforms
317 $Na_V1.3$, $Na_V1.4$, $Na_V1.2$, $Na_V1.1$, and $Na_V1.6$ (in order of abundance) have been detected in
318 neonatal and adult mouse and rat ventricular cardiomyocytes (21, 27, 38, 39). These neuronal
319 and skeletal muscle Na_V isoforms, along with the β1 and β3 auxillary subunits, are primarily

320 located in the transverse tubules whereas the predominantly more abundant cardiac $Na_V1.5$ along
321 with the β1, β2, and β4 subunits preferentially localize to the intercalated disc. The non-cardiac
322 Na_V isoforms may account for up to 30% of cardiac I_{Na} in neonatal rat ventricular myocytes
323 (NRVMs), but account for <10% of total cardiac I_{Na} in isolated adult mouse ventricular
324 myocytes (21, 27). We did not assay for non-cardiac Na_V or β-subunit isoforms in the present
325 study and will consider these transcripts and proteins in future experiments, but the close
326 correlation between the decrease in $Na_V1.5$ protein levels and peak I_{Na} density in our experiments
327 (Figs. 1 and 5) are consistent with the interpretation that the decrease in peak cardiac I_{Na}
328 observed with pan-HDAC inhibition is due to dose-dependent reductions in $Na_V1.5$ protein
329 levels.
330
331 The precise molecular basis for the decrease in $Na_V1.5$ protein expression remains to be
332 determined by future investigations, though downregulation of *Scn5a* expression cannot be ruled
333 out at higher inhibitory concentrations of TSA and VOR. Possible mechanisms for the
334 downregulation of cardiac I_{Na} include variations in the Scn5a transcripts that don't equally
335 translate into functional $Na_V1.5$ protein, microRNA regulation of *Scn5a* transcripts, increased
336 $Na_V1.5$ degradation by Nedd4-2-mediated ubiquitination, and reduced expression of the MOG1
337 protein that directly interacts with and increases the functional surface expression of $Na_V1.5$
338 channels (10, 52, 63, 69). The surface expression and localization of $Na_V1.5$ is also modulated by
339 direct interactions with α-actinin-2, ankyrin-G, glycerol-3-phosphate dehydrogenase 1 like gene
340 (GPD1-L), SAP-97, and tyrosine-phosphorylated β1 (pYb1) and indirect protein-protein
341 interactions with Cx43, N-cadherin (Ncad), the syntrophin-dystrophin complex including
342 calcium/calmodulin-dependent serine kinase (CASK), and plakophilin-2 (PKP2), all of which

343 can result in functional reductions in $Na_V1.5$ expression (12, 25, 35, 41, 46, 48, 51, 52, 54, 68,
344 74). Thus, our findings of reduced Ncad and Cx43 protein levels observed with TSA, VOR, and
345 FK228 are consistent with decreases in I_{Na} (71).
346
347 Besides the many possible direct and indirect protein interactions with $Na_V1.5$, numerous post-
348 translational modifications alter $Na_V1.5$ function including glycosylation, phosphorylation by
349 numerous kinases (e.g. PKA, PKC, CaMKII, Fyn), ubiquitination, S-nitrosylation, and
350 methylation (1, 3, 7, 52, 63). N^{ε}-lysine acetylation directly or indirectly impacts protein
351 methylation, neddylation, ubiquitylation, and phosphorylation either by mutually exclusive post-
352 translational modification (PTM) of lysine residues or lysine residues within concensus protein
353 kinase phosphorylation sites (72). N-terminal acetylation of $Na_V1.5$ was recently discovered in
354 end stage human heart failure and is associated with specific protein degradatory pathways that
355 likely results in the downregulation of cardiac I_{Na} (2, 4, 23, 42). N-terminal (Nt- or N^{α})
356 acetylation is irreversibly catalyzed by ribosome-associated N-terminal acetyltransferases
357 (NATs) and is distinct from the N^{ε}-lysine acetylation reaction catalyzed by the histone
358 acetyltransferases (HATs) and reversed by the HDACs and sirtuins (SIRTs, Class III NAD^+-
359 dependent HDACs) (2, 73). Classical HDAC inhibition will not affect NAT or SIRT activities,
360 although HDAC6 and SIRT2 colocalize to form the tubulin deactylase complex (47). Whether or
361 not $Na_V1.5$ is a substrate for N^{e}-lysine acetylation is currently unknown, so we subjected mouse
362 and human $Na_V1.5$ sequences to N^{e}-lysine acetylation site analysis using the PHOSIDA website
363 (18). This bioinformatic analysis predicted two high probability (>90%) cytoplasmic acetylation
364 sites near the domain II and IV S4 segments known to be involved in V_m-dependent activation
365 (Fig. 7A). To determine if $Na_V1.5$ is acetylated, we injected six adult C57BL/6 mice with 10

mg/kg TSA or DMSO/saline control i.p. injections for 5 days and immunoprecipitated the ventricular heart lysates with anti-$Na_V1.5$ antibodies. Subsequent immunoblotting for acetylated protein with an anti-acetyl-lysine (Ac-K) antibody revealed an increase in acetylated $Na_V1.5$ protein with TSA treatments (Fig. 7B,C). The human and murine $Na_V1.5$ proteins possess 94% sequence identity, hence we hypothesize that acetylation of K830 and K1644 (K1641 in the human sequence) may account for the small depolarizing shift in the I_{Na} activation curve and the slowing of the inactivation rate at low activation potentials seen with pan-HDAC inhibition (Figs. 2 and 3). This postulated acetylation-dependent shift of $Na_V1.5$ activation decreased the V_m-dependent window for prolonged activation of I_{Na} (window current) and is unlikely to account for the observed decrease results in I_{Na} density, which correlates closely with the decreased levels of $Na_V1.5$ protein. Identification of the actual $Na_V1.5$ acetylation sites will require future liquid chromatography-electron spray ionization tandem mass spectroscopic analyses of IP-enriched and/or SDS-PAGE proteolytic $Na_V1.5$ peptide digests (32).

There are nearly 500 $Na_V1.5$ mutations associated with cardiac arrhythmias including long QT (LQT3) syndrome, Brugada syndrome (BrS), cardiac conduction disease (CCD), sick sinus syndrome (SSS), and atrial fibrillation (AF) (13, 40, 51, 52, 65, 75). $Na_V\beta1$-4 subunits also contribute to LQT and AF cardiac arrhythmias (43, 66, 67). Approximately 75% of these mutations cause loss of $Na_V1.5$ function except those involved in LQT and some AF arrhythmias. Gain-of-function $Na_V1.5$ mutations typically increase activation or decrease inactivation, resulting in a net increase of a persistent (sustained) or late I_{Na} that prolongs action potential duration and enhances the occurrence of early afterdepolarizations (EADs) (43, 65). For example, expression of the $Na_V1.5$F1486del LQT mutation increased late I_{Na} and produced

389 EADs in NRVMs (59). Recently, increased expression of $Na_V1.1$ and $Na_V1.3$ isoforms in
390 *Scnb1*$^{-/-}$ mice and ischemic heart failure dog hearts produced increases in late I_{Na} and
391 arrhythmias, thus indicating a role for neuronal isoforms in cardiac arrhythmogenesis (33, 44).
392 However, we found no evidence for pan-HDAC inhibitor-induced increase in late I_{Na} in NMVMs
393 or hiPSC-CMs. By contrast, loss-of-function mutations shorten the cardiac refractory period and
394 slow conduction velocity leading to arrhythmias including BrS, SSS, and CCD (6, 56, 61, 67).
395 Peak I_{Na} density and gap junction conductance (g_j) are primary determinants of myocardial
396 conduction velocity and reductions in both of these factors will slow conduction and increase the
397 vulnerability to reentrant arrhythmias (30, 62). BrS arrhythmias frequently develop in the right
398 ventricle which is more susceptible to conduction slowing secondary to $Na_V1.5$ dysfunction (49,
399 51).
400
401 All three pan-HDAC inhibitors we have tested thus far caused significant reductions in g_j and
402 I_{Na}, consistent with an increased susceptibility to cardiac arrhythmias due to slowed or
403 discontinuous propagation (71). Reduced gap junction coupling also enhances the ability of
404 triggered afterdepolarizations to initiate an arrhythmia including LQT-induced TdP arrhythmias
405 by modulating the source-sink interactions of an ectopic focus with the surrounding normal
406 myocardium (53, 70). Enhancement of late I_{Na} currents and blockade of repolarizing delayed
407 outward K^+ currents account for >90% of all congenital and drug-induced LQT syndromes (26).
408 However, the IC_{50} for VOR blockade of the rapid delayed outward rectifying K^+ current (I_{Kr})
409 formed by the hERG and MiRP1 channel and accessory proteins is 300 μM, orders of magnitude
410 higher than the recommended therapeutic dose of 1 μM (29). Thus, direct hERG blockade is
411 unlikely to account for the observed QT interval prolongation and *Torsades de Pointes* (TdP)

arrhythmias occasionally observed with this HDAC inhibitor (36, 50). Two recent studies have concluded that the cardiotoxic effects of HDAC inhibitors likely results from transcriptional changes in genes affecting ion channel function owing to their delayed onset of cardiotoxicity and lack of acute ion channel blockade (31, 60). Owing to the present and recent findings, identification of the ionic mechanisms responsible for HDAC inhibitor-induced QT interval prolongation and TdP arrhythmias merits further investigation. In conclusion, pan-HDAC-induced reductions in peak cardiac I_{Na} and $Na_V1.5$ protein levels and shifted the activation curve positive, possibly due to direct acetylation of two S4 segment adjacent cytoplasmic lysine residues. These effects on I_{Na} should decrease cardiac excitability, refractoriness, and conduction velocity in a manner that will increase myocardial vulnerability to reentrant arrhythmias, but not LQT-associated *Torsades de Pointes* arrhythmias that occasionally occur with pan-HDAC inhibitory treatments.

Acknowledgements

We wish to thank Li Gao for her technical assistance during the performance of this work.

Dr. Qin Xu's current address is: Department of Psychiatry, Faculty of Medicine The University of British Columbia, 2255 Wesbrook Mall, Vancouver, B.C. V6T 1Z3, Canada Tel: 604-822-7383.

Grants

Grant support for this work was provided by the National Heart, Lung, and Blood Institute of the National Institutes of Health (HL042220), the Joseph C Georg Fund of the Central New York Community Foundation/Upstate Medical University Foundation, and the Hendricks Fund of the Health Science Center Foundation at Syracuse to R.D.V.

435 **References**

436 (1) **Ahern GP, Hsu SF, Klyachko VA, Jackson MB.** Induction of persistent sodium current by
437 exogenous and endogenous nitric oxide. *J Biol Chem* 275: 28810–28815, 2000.
438 (2) **Arnesen T.** Towards a functional understanding of protein N-terminal acetylation. *PLoS Biol*
439 9(5): e1001074, 2011. doi:10.1371/journal.pbio.1001074
440 (3) **Beltran-Alvarez P, Pagans S, Brugada R.** The cardiac sodium channel is post-
441 translationally modified by arginine methylation. *J Proteome Res* 10: 3712-3719, 2011.
442 (4) **Beltran-Alvarez P, Tarradas A, Chiva C, Pérez-Serra A, Batlle M, Pérez-Villa F,**
443 **Schulte U, Sabidó E, Brugada R, Pagans S.** Identification of N-terminal protein acetylation
444 and arginine methylation of the voltage-gated sodium channel in end-stage heart failure human
445 heart. *J Mol Cell Cardiol* 76: 126-129, 2014.
446 (5) **Bradner JE, West N, Grachan ML, Greenberg EF, Haggarty SJ, Warnow T,**
447 **Mazitschek R.** Chemical phylogenetics of histone deacetylases. *Nat Chem Biol* 6: 238-243,
448 2010.
449 (6) **Chen Q, Kirsch GE, Zhang D, Brugada R, Brugada J, Brugada P, Potenza D, Moya A,**
450 **Borggrefe M, Breithardt G, Ortiz-Lopez R, Wang Z, Antzelevitch C, O'Brien RE, Schulze-**
451 **Bahr E, Keating MT, Towbin JA, Wang Q.** Genetic basis and molecular mechanism for
452 idiopathic ventricular fibrillation. *Nature* 392: 293–296, 1998.
453 (7) **Cheng J, Valdivia CR, Vaidyanathan R, Balijepalli RC, Ackerman MJ, Makielski JC.**
454 Caveolin-3 suppresses late sodium current by inhibiting nNOS-dependent S-nitrosylation of
455 SCN5A. *J Mol Cell Cardiol* 61: 102-110, 2013.
456 (8) **Colussi C, Berni R, Rosati J, Straino S, Vitale S, Spallotta F, Baruffi S, Bocchi L,**
457 **Delucchi F, Rossi S, Savi M, Rotili D, Quaini F, Macchi E, Stilli D, Musso E, Mai A,**

Gaetano C, Capogrossi MC. The histone deacetylase inhibitor suberoylanilide hydroxamic acid reduces cardiac arrhythmias in dystrophic mice. *Cardiovasc Res* 87: 73-82, 2010.

(9) **Colussi C, Rosati J, Straino S, Spallotta F, Berni R, Stilli D, Rossi S, Musso E, Macchi E, Mai A, Sbardella G, Castellano S, Chimenti C, Frustaci A, Nebbioso A, Altucci L, Capogrossi MC, Gaetano C.** N^{ε}-lysine acetylation determines dissociation from gap junctions and lateralization of connexin 43 in normal and dystrophic heart. *Proc Natl Acad Sci USA* 108:2795-2800, 2011.

(10) **Daimi H, Lozano-Velasco E, Haj Khelil A, Chibani JB, Barana A, Amorós I, González de la Fuente M, Caballero R, Aranega A, Franco D.** Regulation of SCN5A by microRNAs: miR-219 modulates SCN5A transcript expression and the effects of flecainide intoxication in mice. *Heart Rhythm* 12: 1333-1342, 2015.

(11) **Dasmahapatra G, Patel H, Friedberg J, Quayle SN, Jones SS, Grant S.** In vitro and in vivo interactions between the HDAC6 inhibitor ricolinostat (ACY1215) and the irreversible proteasome inhibitor carfilzomib in non-Hodgkin lymphoma cells. *Mol Cancer The.* 13: 2886-2897, 2014.

(12) **Eichel CA, Beuriot A, Chevalier M, Rougier JS, Louault F, Dilanian G, Amour J, Coulombe A, Abriel H, Hatem SN, Balse E.** Lateral membrane-specific MAGUK CASK down-regulates NaV1.5 channel in cardiac myocytes. *Circ Res* 119: 544-556, 2016.

(13) **Ellinor PT, Nam EG, Shea MA, Milan DJ, Ruskin JN, MacRae CA.** Cardiac sodium channel mutation in atrial fibrillation. *Heart Rhythm* 5: 99-105, 2008.

(14) FDA Reference ID 3043460, 3536712, 3643827, and 3699607.

(15) **Foss F, Advani R, Duvic M, Hymes KB, Intragumtornchai T, Lekhakula A, Shpilberg O, Lerner A, Belt RJ, Jacobsen ED, Laurent G, Ben-Yehuda D, Beylot-Barry M, Hillen U,**

Knoblauch P, Bhat G, Chawla S, Allen LF, Pohlman B. A Phase II trial of Belinostat (PXD101) in patients with relapsed or refractory peripheral or cutaneous T-cell lymphoma. *Br J Haematol* 168: 811-819, 2015.

(16**) Gavillet B, Rougier JS, Domenighetti AA, Behar R, Boixel C, Ruchat P, Lehr HA, Pedrazzini T, Abriel H**. Cardiac sodium channel Nav1.5 is regulated by a multiprotein complex composed of syntrophins and dystrophin. *Circ Res* 99: 407–414, 2006.

(17) **Giles F, Fischer T, Cortes J,Garcia-Manero G, Beck J, Ravandi F, Masson E, Rae P, Laird G, Sharma S, Kantarjian H, Dugan M, Albitar M, and Bhalla K.** A phase I study of intravenous LBH589, a novel cinnamic hydroxamic acid analogue histone deacetylase inhibitor, in patients with refractory hematologic malignancies. *Clin Cancer Res* 12: 4628-4635, 2006.

(18) **Gnad F, Gunawardena J, Mann M.** PHOSIDA 2011: the posttranslational modification database. *Nucleic Acid Res* 39(Suppl 1): D253-D260, 2011.

(19) **Gryder BE, Sodji QH, Oyelere AK.** Targeted cancer therapy: giving histone deacetylase inhibitors all they need to succeed. *Future Med Chem* 4: 505-524, 2012.

(20) **Haberland M, Montgomery RL, and Olson EN.** The many roles of histone deacetylases in development and physiology: implication for disease and therapy. *Nat Rev Genetics* 10: 32-42, 2009.

(21) **Haufe V, Camacho JA, Dumaine R, Günther B, Bollensdorff C, von Banchet GS, Benndorf K, Zimmer T.** Expression pattern of neuronal and skeletal muscle voltage-gated Na+ channels in the developing mouse heart. *J Physiol* 564: 683-696, 2005.

(22) **Heerboth S, Lapinska K, Snyder N, Leary M, Rollinson S, Sarkar S.** Use of epigenetic drugs in disease: an overview. *Genet Epigenet* 6: 9-19, 2014.

(23) **Hwang CS, Shemorry A, Varshavsky A.** N-terminal acetylation of cellular proteins creates specific degradation signals. *Science* 327: 973–977, 2010.

(24) **Iyer A, Fairlie DP, Brown L.** Lysine acetylation in obesity, diabetes and metabolic disease. *Immunol Cell Biol* 90: 39-46, 2012.

(25) **Jansen JA, Noorman M, Musa H, Stein M, de Jong S, van der Nagel R, Hund TJ, Mohler PJ, Vos MA, van Veen TA, de Bakker JM, Delmar M, van Rijen HV.** Reduced heterogeneous expression of Cx43 results in decreased Nav1.5 expression and reduced sodium current that accounts for arrhythmia vulnerability in conditional Cx43 knockout mice. *Heart Rhythm* 9: 600-607, 2012.

(26) **Kannankeril P, Roden DM, Darbar D.** Drug-induced long QT syndrome. *Pharmacol Rev* 62: 760-781, 2010.

(27) **Kaufmann SG, Westenbroek RE, Zechner C, Maass AH, Bischoff S, Muck J, Wischmeyer E, Scheuer T, Maier SK.** Functional protein expression of multiple sodium channel alpha- and beta-subunit isoforms in neonatal cardiomyocytes. *J Mol Cell Cardiol* 48: 261-269, 2010.

(28) **Kazantsev AG, and Thompson LM.** Therapeutic application of histone deaceytlase inhibitors for central nervous system disorders. *Nat Rev Drug Disc* 2008;7:854-868.

(29) **Kerr JS, Galloway S, Lagrutta A, Armstrong M, Miller T, Richon VM, Andrews PA.** Nonclinical safety assessment of the histone deacetylase inhibitor vorinostat. *Intl J Toxicol* 29: 3-19, 2010.

(30) **Kléber AG, Rudy Y.** Basic mechanisms of cardiac impulse propagation and associated arrhythmias. *Physiol Rev* 84:431-488, 2003.

(31) **Kopljar I, Gallacher DJ, De Bondt A, Cougnaud L, Vlaminckx E, Van den Wyngaert I, Lu HR.** Functional and transcriptional characterization of histone deacetylase inhibitor-mediated cardiac adverse effects in human induced pluripotent stem cell-derived cardiomyocytes. *Stem Cells Transl Med* 5: 602-612, 2016.

(32) **Li Y, Silva JC, Skinner ME, Lombard DB.** Mass spectrometry-based detection of protein acetylation. *Methods Mol Biol* 1077: 81-104, 2013.

(33) **Lin X, O'Malley H, Chen C, Auerbach D, Foster M, Shekhar A, Zhang M, Coetzee W, Jalife J, Fishman GI, Isom L, Delmar M.** Scn1b deletion leads to increased tetrodotoxin-sensitive sodium current, altered intracellular calcium homeostasis and arrhythmias in murine hearts. *J Physiol* 593: 1389-1407, 2015.

(34) **Lobera M, Madauss KP, Pohlhaus DT, Wright QG, Trocha M, Schmidt DR, Baloglu E, Trump RP, Head MS, Hofmann GA, Murray-Thompson M, Schwartz B, Chakravorty S, Wu Z, Mander PK, Kruidenier L, Reid RA, Burkhart W, Turunen BJ, Rong JX, Wagner C, Moyer MB, Wells C, Hong X, Moore JT, Williams JD, Soler D, Ghosh S, Nolan MA.** Selective class IIa histone deacetylase inhibition via a nonchelating zinc-binding group. *Nat Chem Biol* 9: 319-325, 2013.

(35) **London B, Michalec M, Mehdi H, Zhu X, Kerchner L, Sanyal S, Viswanathan PC, Pfahnl AE, Shang LL, Madhusudanan M, Baty CJ, Lagana S, Aleong R, Gutmann R, Ackerman MJ, McNamara DM, Weiss R, Dudley SC Jr.** Mutation in glycerol-3-phosphate dehydrogenase 1 like gene (GPD1-L) decreases cardiac Na^+ current and causes inherited arrhythmias. *Circulation* 116: 2260-2268, 2007.

(36) **Lynch DR, Washam JB, Newby LK.** QT interval prolongation and torsades de pointes in a patient undergoing treatment with vorinostat: A case report and review of the literature. *Cardiol J* 19: 434-438, 2012.

(37) **Ma J, Guo L, Fiene SJ, Anson BD, Thomson JA, Kamp TJ, Kolaja KL, Swanson BJ, January CT.** High purity human-induced pluripotent stem cell-derived cardiomyocytes: electrophysiological properties of action potentials and ionic currents. *Am J Physiol Heart Circ Physiol* 301: H2006-H2017, 2011.

(38) **Maier SK, Westenbroek RE, McCormick KA, Curtis R, Scheuer T, Catterall WA.** Distinct subcellular localization of different sodium channel alpha and beta subunits in single ventricular myocytes from mouse heart. *Circulation* 109: 1421-1427, 2004.

(39) **Maier SK, Westenbroek RE, Schenkman KA, Feigl EO, Scheuer T, Catterall WA.** An unexpected role for brain-type sodium channels in coupling of cell surface depolarization to contraction in the heart. *Proc Natl Acad Sci U S A* 99: 4073-4078, 2002.

(40) **Makiyama T, Akao M, Shizuta S, Doi T, Nishiyama K, Oka Y, Ohno S, Nishio Y, Tsuji K, Itoh H, Kimura T, Kita T, Horie M.** A novel SCN5A gain-of-function mutation M1875T associated with familial atrial fibrillation. *J Am Coll Cardiol* 52(16):1326-1334, 2008.

(41) **Malhotra JD, Thyagarajan V, Chen C, Isom LL.** Tyrosine-phosphorylated and nonphosphorylated sodium channel beta1 subunits are differentially localized in cardiac myocytes. *J Biol Chem* 279: 40748-40754, 2004.

(42) **Marionneau C, Abriel H.** Regulation of the cardiac Na+ channel NaV1.5 by post-translational modifications. *J Mol Cell Cardiol* 82:36-47, 2015.

(43) **Medeiros-Domingo A, Kaku T, Tester DJ, Iturralde-Torres P, Itty A, Ye B, Valdivia C, Ueda K, Canizales-Quinteros S, Tusié-Luna MT, Makielski JC, Ackerman MJ.** SCN4B-

encoded sodium channel beta4 subunit in congenital long-QT syndrome. *Circulation* 116: 134–142, 2007.

(44) **Mishra S, Reznikov V, Maltsev VA, Undrovinas NA, Sabbah HN, Undrovinas A.** Contribution of sodium channel neuronal isoform Nav1.1 to late sodium current in ventricular myocytes from failing hearts. *J Physiol* 593: 1409-1427 2015.

(45) **Mogal A, Abdulkadir SA.** Effects of Histone Deacetylase Inhibitor (HDACi); Trichostatin-A (TSA) on the expression of housekeeping genes. *Molec Cell Probes* 20: 81-86, 2006.

(46) **Noorman M, Hakim S, Kessler E, Groeneweg JA, Cox MG, Asimaki A, van Rijen HV, van Stuijvenberg L, Chkourko H, van der Heyden MA, Vos MA, de Jonge N, van der Smagt JJ, Dooijes D, Vink A, de Weger RA, Varro A, de Bakker JM, Saffitz JE, Hund TJ, Mohler PJ, Delmar M, Hauer RN, van Veen TA**. Remodeling of the cardiac sodium channel, connexin43, and plakoglobin at the intercalated disk in patients with arrhythmogenic cardiomyopathy. *Heart Rhythm* 10: 412-419, 2013.

(47) **North BJ, Marshall BL, Borra MT, Denu JM, Verdin E.** The human Sir2 ortholog, SIRT2, is an NAD+-dependent tubulin deacetylase. *Mol Cell* 11: 437-444, 2003.

(48) **Petitprez S, Zmoos AF, Ogrodnik J, Balse E, Raad N, El-Haou S, Albesa M, Bittihn P, Luther S, Lehnart SE, Hatem SN, Coulombe A, Abriel H.** SAP97 and dystrophin macromolecular complexes determine two pools of cardiac sodium channels Nav1.5 in cardiomyocytes. *Circ Res* 108: 294-304, 2011.

(49) **Postema PG, van Dessel PF, de Bakker JM, Dekker LR, Linnenbank AC, Hoogendijk MG, Coronel R, Tijssen JG, Wilde AA, Tan HL.** Slow and discontinuous conduction conspire in Brugada syndrome: a right ventricular mapping and stimulation study. *Circ Arrhythm Electrophysiol* 1: 379-386, 2008.

(50) **Rasheed WK, Johnstone RW, Price HM.** Histone deacetylase inhibitors in cancer therapy. *Expert Opin Invest Drugs* 16: 659-678, 2007.

(51) **Remme CA, Bezzina CR.** Sodium channel (dys)function and cardiac arrhythmias. *Cardiovasc Ther* 28: 287-294, 2010.

(52) **Rook MB, Evers MM, Vos MA, Bierhuizen MF.** Biology of cardiac sodium channel Nav1.5 expression. *Cardiovasc Res* 93: 12-23, 2012.

(53) **Ruan L, Quan X, Li L, Bai R, Ni M, Xu R, Zhang C.** Increasing gap junction coupling supresses ibutilide-induced torsades de pointes. *Exp Ther Med* 7: 1279-1284, 2014.

(54) **Sato PY, Musa H, Coombs W, Guerrero-Serna G, Patiño GA, Taffet SM, Isom LL, Delmar M.** Loss of plakophilin-2 expression leads to decreased sodium current and slower conduction velocity in cultured cardiac myocytes. *Circ Res* 105: 523-526, 2009.

(55) **Schiattarella GG, Sannino A, Toscano E, Cattaneo F, Trimarco B, Esposito G, Perrino C.** Cardiovascular effects of histone deacetylase inhibitors epigenetic therapies: Systematic review of 62 studies and hypotheses for future research. *Int J Cardiol* 219: 396-403, 2016.

(56) **Schott JJ, Alshinawi C, Kyndt F, Probst V, Hoorntje TM, Hulsbeek M, Wilde AA, Escande D, Mannens MM, Le Marec H.** Cardiac conduction defects associate with mutations in SCN5A. *Nat. Genet* 23: 20–21, 1999.

(57) **Shah MH, Binkley P, Chan K, Xiao J, Arbogast D, Collamore M, Farra Y, Young D, Grever M.** Cardiotoxicity of histone deacetylase inhibitor depsipeptide in patients with metastatic neuroendocrine tumors. *Clin Cancer Res* 12: 3997-4003, 2006.

(58) **Shakespear, M. R., Halili, M. A., Irvine, K. M., Fairlie, D. P., Sweet, M.J.** Histone deacetylases as regulators of inflammation and immunity. *Trends Immunol* 32: 335-343, 2011.

(59) **Song W, Xiao Y, Chen H, Ashpole NM, Piekarz AD, Ma P, Hudmon A, Cummins TR, Shou W.** The human Nav1.5 F1486 deletion associated with long QT syndrome leads to impaired sodium channel inactivation and reduced lidocaine sensitivity. *J Physiol* 590: 5123-5139, 2012.

(60) **Spence S, Deurinck M, Ju H, Traebert M, McLean L, Marlowe J, Emotte C, Tritto E, Tseng M, Shultz M, Friedrichs GS**. Histone deacetylase inhibitors prolong cardiac repolarization through transcriptional mechanisms. *Toxicol Sci* 2016 Jun 2. pii: kfw104, 2016.

(61) **Tan HL, Bink-Boelkens MT, Bezzina CR, Viswanathan PC, Beaufort-Krol GC, van Tintelen PJ, van den Berg MP, Wilde AA, Balser JR.** A sodium-channel mutation causes isolated cardiac conduction disease. *Nature* 409: 1043–1047, 2001.

(62) **Tse G, Yeo JM.** Conduction abnormalities and ventricular arrhythmogenesis: The roles of sodium channels and gap junctions. *Int J Cardiol Heart Vasc* 7;9: 75-82, 2015.

(63) **van Bemmelen MX, Rougier JS, Gavillet B, Apothéloz F, Daidié D, Tateyama M, Rivolta I, Thomas MA, Kass RS, Staub O, Abriel H**. Cardiac voltage-gated sodium channel Nav1.5 is regulated by Nedd4-2 mediated ubiquitination. *Circ Res* 95: 284-291, 2004.

(64) **Veenstra RD.** Voltage clamp limitations of dual whole cell recordings of gap junction current and voltage recordings. I. Conductance measurements. *Biophys J* 80: 2231-2247, 2001.

(65) **Wang Q, Shen J, Splawski I, Atkinson D, Li Z, Robinson JL, Moss AJ, Towbin JA, Keating MT.** SCN5A mutations associated with an inherited cardiac arrhythmia, long QT syndrome. *Cell* 80: 805–811, 1995.

(66) **Watanabe H, Darbar D, Kaiser DW, Jiramongkolchai K, Chopra S, Donahue BS, Kannankeril PJ, Roden DM.** Mutations in sodium channel β1- and β2-subunits associated with atrial fibrillation. *Circ Arrhythm Electrophysiol* 2: 268-75, 2009.

(67) **Watanabe H, Koopmann TT, Le Scouarnec S, Yang T, Ingram CR, Schott JJ, Demolombe S, Probst V, Anselme F, Escande D, Wiesfeld AC, Pfeufer A, Kääb S, Wichmann HE, Hasdemir C, Aizawa Y, Wilde AA, Roden DM, Bezzina CR.** Sodium channel β1 subunit mutations associated with Brugada syndrome and cardiac conduction disease in humans. *J Clin Invest* 118: 2260-2268, 2008.

(68) **Willis BC, Ponce-Balbuena D, Jalife J.** Protein assemblies of sodium and inward rectifier potassium channels control cardiac excitability and arrhythmogenesis. *Am J Physiol Heart Circ Physiol* 15;308: H1463-H1473, 2015.

(69) **Wu L, Yong SL, Fan C, Ni Y, Yoo S, Zhang T, Zhang X, Obejero-Paz CA, Rho HJ, Ke T, Szafranski P, Jones SW, Chen Q, Wang QK.** Identification of a new co-factor, MOG1, required for the full function of cardiac sodium channel Nav 1.5. *J Biol Chem* 283: 6968-6978, 2008.

(70) **Xie Y, Sato D, Garfinkel A, Qu Z, Weiss JN.** So little source, so much sink: requirements for afterdepolarizations to propagate in tissue. *Biophys J* 99: 1408-1415, 2010.

(71) **Xu Q, Lin X, Andrews L, Patel D, Lampe PD, Veenstra RD.** Histone deacetylase inhibition reduces cardiac connexin43 expression and gap junction communication. *Front Pharmacol* 4:44, 2013. doi: 10.3389/fphar.2013.00044.

(72)**Yang XJ, Grégoire S.** Metabolism, cytoskeleton and cellular signalling in the grip of protein Nepsilon - and O-acetylation. *EMBO Rep* 8: 556-562 2007.

(73) **Yang XJ, Seto E.** The Rpd3/Hda1 family of lysine deacetylases: from bacteria and yeast to mice and men. *Nat Rev Mol Cell Biol* 9: 206-218, 2008.

(74) **Ziane R, Huang H, Moghadaszadeh B, Beggs AH, Levesque G, Chahine M.** Cell membrane expression of cardiac sodium channel Na(v)1.5 is modulated by alpha-actinin-2 interaction. *Biochemistry* 49: 166-178, 2010..

(75) **Zimmer T, Haufe V, Blechschmidt S.** Voltage-gated sodium channels in the mammalian heart. *Glob Cardiol Sci Pract* 2014: 449-463, 2014.

664 **Figure Captions**

665 **Figure 1.** Reduction of Cardiac I_{Na} by pan-HDAC inhibition. Families of cardiac Na^+ current
666 traces are shown for 10 mV depolarizing voltage clamp steps from -90 to +50 mV under control
667 (A), 100 nM trichostatin A (TSA, B), 5 μM vorinostat (VOR, C), and 10 nM romidepsin
668 (FK228, D). (E) Diagram of the V_m pulse protocol for activating I_{Na}. (F-H) I_{Na} current density
669 (pA/pF) – V_m relationships under control conditions and after 18-24 hr treatment with 50 or 100
670 nM TSA (F), 1 or 5 μM VOR (G), and 10 nM FK228 (H) illustrate dose-dependent decreases in
671 peak I_{Na} with pan-HDAC inhibitor treatments.

672

673 **Figure 2.** Shift of I_{Na} activation by pan-HDAC inhibition. (A-C) The apparent shift in V_m-
674 dependent activation present in the I-V curves in Figs. 1D-F was examined by calculating the
675 Na^+ conductance (g_{Na}) and normalizing the data to the maximum gNa ($\bar{g}$ Na) for each
676 experimental group and plotting the activation curves for TSA (A), VOR (B), and FK228 (C)
677 relative to the control activation curve. The data points were fitted with a Boltzmann function
678 with a half-activation voltage ($V_{½act}$) of -49.8 mV for control, -46.6 and -47.0 mV for 50 and 100
679 nM TSA, -46.0 and -42.3 mV for 1 and 5 μM VOR, and -46.2 mV for 10 nM FK228,
680 respectively. (D) V_m-dependent inactivation was assessed using a prepulse protocol illustrated in
681 panel (E) and no shift in the half-inactivation voltage ($V_{½inact}$) of -83.0 ± 0.5 mV was observed
682 between control, 100 nM TSA, and 5 μM VOR conditions. (F) Comparison of the overlap
683 between the g_{Na} inactivation and activation curves under control and 5 μM VOR illustrating the
684 decrease in the V_m-dependent "window" for persistent activation of I_{Na}.

685

686 **Figure 3.** I_{Na} inactivation time constants. (A-C) The average V_m-dependent inactivation time
687 constants (τ_h) from the control, 100 nM TSA (A), 1 μM VOR (B), and 10 nM FK228 (C) I_{Na}
688 current traces illustrate only a slight slowing of the inactivation rates at low activating potentials
689 of -60 to -40 mV with no slowing of inactivation at fully activated potentials > -40 mV.
690
691 **Figure 4.** Effect of pan-HDAC inhibition on human I_{Na}. (A and B) Examples of a family of I_{Na}
692 traces obtained from a human induced-pluripotent stem cell-derived cardiomyocyte (hiPSC-CM)
693 under control (A) and 1 μM VOR (B) conditions. (C) I_{Na} current density (pA/pF) – V_m
694 relationships under control conditions and 1 μM VOR conditions illustrate a significant
695 reduction in I_{Na} density after pan-HDAC inhibitor treatment, verifying previous results obtained
696 from NMVM cultures.
697
698 **Figure 5.** Effects of pan-HDAC inhibition on $Na_V1.5$ expression. (A) The abundance of mRNA
699 levels were measured by RT-PCR from high density NMVM cultures under control conditions
700 for the Cx43 (*Gja1*), $Na_V1.5$ (*Scn5a*), N-cadherin (*Cdh2*), and the sodium-calcium exchanger
701 (NCX, *Slc8a*) genes relative to *Gapdh*. (B) The relative mRNA levels for these same cardiac
702 genes after 1 μM VOR treatment were compared to control values and only *Gja1* and *Cdh2*
703 levels were significantly reduced as previously reported. The *Gapdh* levels were not significantly
704 different from control values ($p > 0.25$, paired t-test). (C) Representative Western blots for
705 $Na_V1.5$ protein from TSA and VOR treated NMVM samples. HDAC1 was used as loading
706 control and acetylated α-tubulin (Ac-α-t) as an indicator of increased protein acetylation. The
707 experiments were performed in triplicate. (D) Densitometric scans of the Western blot data was
708 performed to quantify the $Na_V1.5$ protein levels at low and high doses of TSA and VOR. $Na_V1.5$

protein levels were significantly reduced at both doses of TSA and VOR. (E) The relative mRNA levels for the *Slc8a*, *Gja1* and *Cdh2* genes were significantly reduced by 10 nM FK228 treatment compared to control values but the Scn5a levels were not significantly affected.

Figure 6. Romidepsin inhibition of cardiac HDAC activity and gap junction conductance. (A) Total HDAC activity was measured in NMVM cultures exposed to increasing concentrations of FK228 using the deacetylated Fluor-de-Lys® fluorescence method. All data were normalized to the background subtracted maximum relative fluorescence of the control well. The data from three experiments were averaged and fitted with a second-order exponential decaying function and equilibrium inhibition constants (K_I) were calculated from the decay constant for each exponential component. (B) The gap junction conductance (g_j) was measured in NMVM cell pairs from control and FK228-treated culture dishes and a dose-dependent decrease in g_j was observed, consistent with published results with TSA and VOR (71).

Figure 7. (A) Putative N^{ε}-lysine acetylation sites on the $Na_V1.5$ Na^+ channel subunit. The full length mouse $Na_V1.5$ amino acid sequence was analyzed for possible lysine acetylation (Ac-K) sites using the prediction algorithm available at the PHOSIDA Posttranslational Modification database (http://www.phosida.org; 18). Eight putative acetylation sites (probability > 90%) were identified and mapped onto the membrane topological model for the $Na_V1.5$ channel protein. Six of the eight predicted $Na_V1.5$ Ac-K sites (K158, K175, K767, K863, K1362, and K1617) mapped to transmembrane or extracellular domain locations and were discounted as possible acetylation sites (⊘). Two possible Ac-K sites, K830 and K1644, mapped to cytoplasmic domains located near the cytoplasmic C-terminal side of the repeat domain II and IV S4 domains

(✸). We hypothesize that acetylation of these two sites, which are conserved in the human $Na_V1.5$ sequence, may account for the slight positive voltage shift (< 10 mV) in the cardiac I_{Na} activation curve associated with pan-HDAC inhibitor treatments (Figs. 2A-C). (B) Left panel, an example of an immunoprecipitation (IP) performed on saline:DMSO (control, C) or TSA-injected (T) mouse heart ventricular lysates with anti-$Na_V1.5$-Protein G magnetic beads and immunoblotted with an anti-acetyl-Lysine (Ac-K) antibody to detect protein acetylation. TSA injection for 5 days caused a dramatic increase in the acetylated $Na_V1.5$ band. Rabbit IgG controls for Control (IgGc) and TSA heart samples (IgGt) are shown in the right two lanes. Right panel, the left two lanes are the $Na_V1.5$ immunoprecipitate input controls for the Control and TSA heart lysates and the right two lanes are the rabbit IgG controls for each sample. (C) Normalized mean Ac-K $Na_V1.5$ band densities for the upper (high molecular weight, MW, upper arrow) and lower (lower MW, lower arrow) from three Control:TSA immunoprecipitation experiments as illustrated in (B). Each Ac-K TSA band density was divided the Control band density for each experiment and this TSA/Control band ratio was normalized by dividing by the $Na_V1.5$ input TSA/Control band ratio.

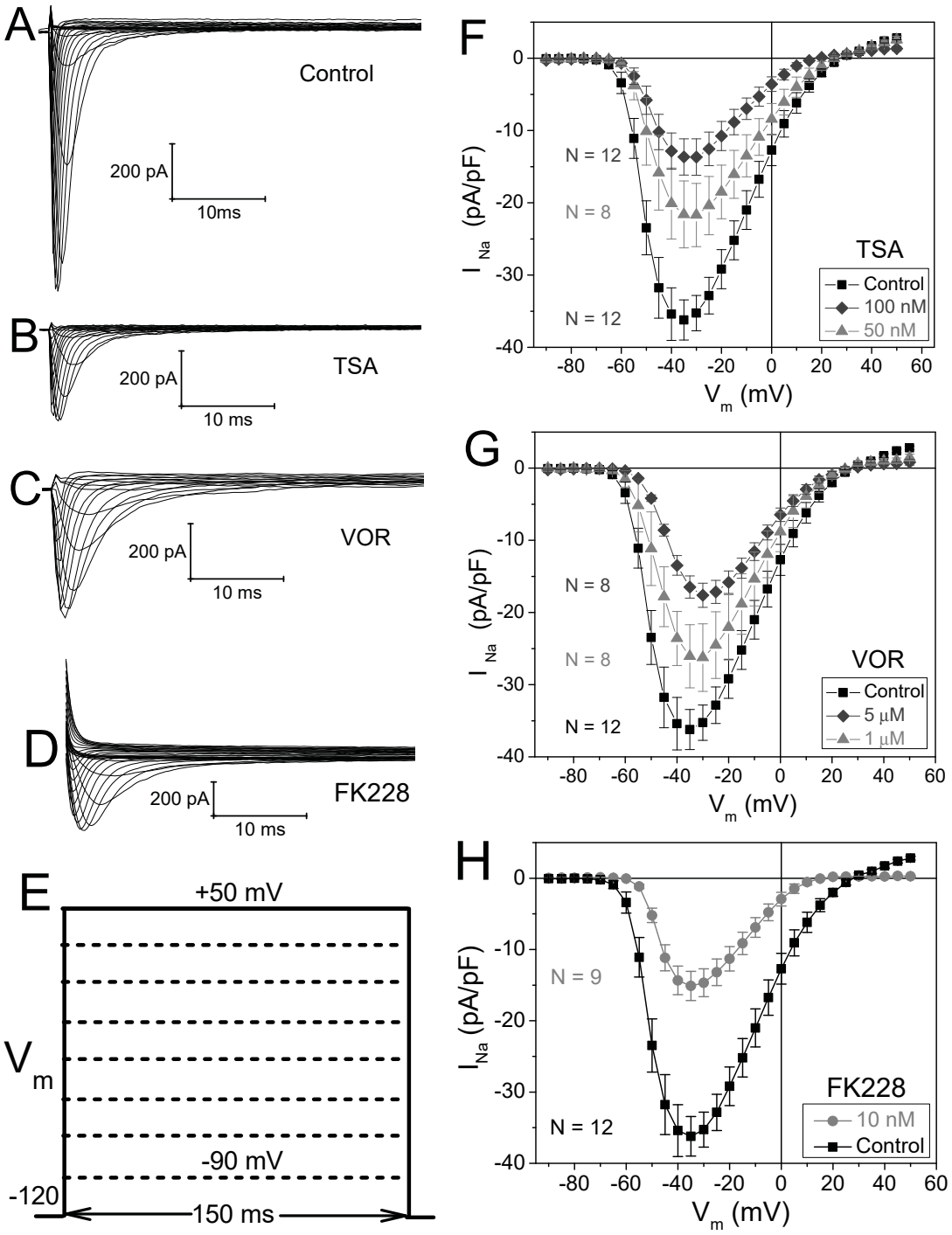
A
Control
200 pA
10ms
B
TSA
200 pA
10 ms
C
VOR
200 pA
10 ms
D
FK228
200 pA
10 ms
E
+50 mV
V m
-90 mV
-120
150 ms
F
N = 12
N = 8
N = 12
I Na (pA/pF)
TSA
Control
100 nM
50 nM
V m (mV)
G
N = 8
N = 8
N = 12
I Na (pA/pF)
VOR
Control
5 μM
1 μM
V m (mV)
H
N = 9
N = 12
I Na (pA/pF)
FK228
10 nM
Control
V m (mV)

Figure 1

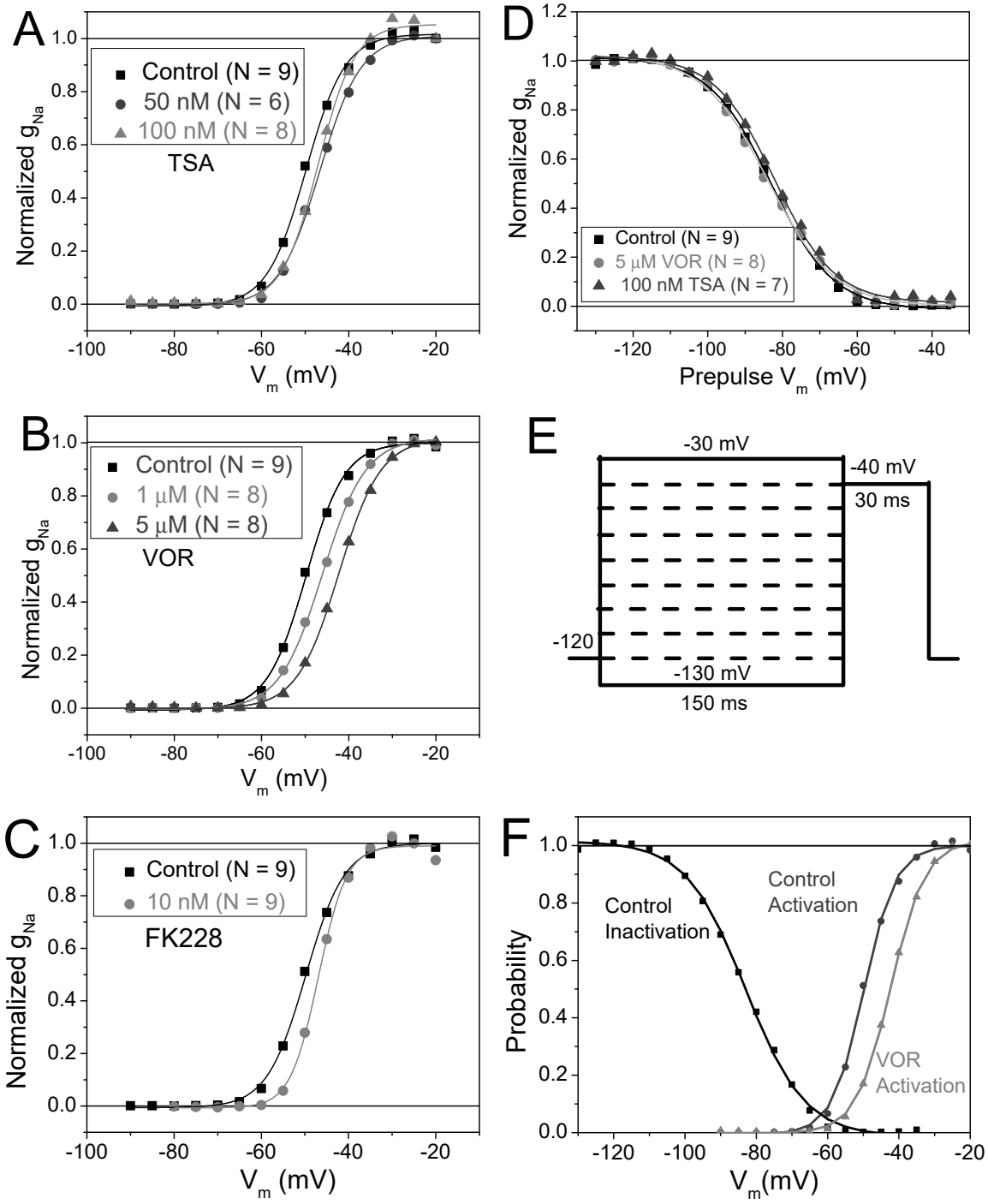
A
Control (N = 9)
50 nM (N = 6)
100 nM (N = 8)
TSA
Normalized g_{Na}
V_m (mV)
B
Control (N = 9)
1 μM (N = 8)
5 μM (N = 8)
VOR
Normalized g_{Na}
V_m (mV)
C
Control (N = 9)
10 nM (N = 9)
FK228
Normalized g_{Na}
V_m (mV)
D
Control (N = 9)
5 μM VOR (N = 8)
100 nM TSA (N = 7)
Normalized g_{Na}
Prepulse V_m (mV)
E
-30 mV
-40 mV
30 ms
-120
-130 mV
150 ms
F
Control Inactivation
Control Activation
VOR Activation
Probability
V_m(mV)

Figure 2

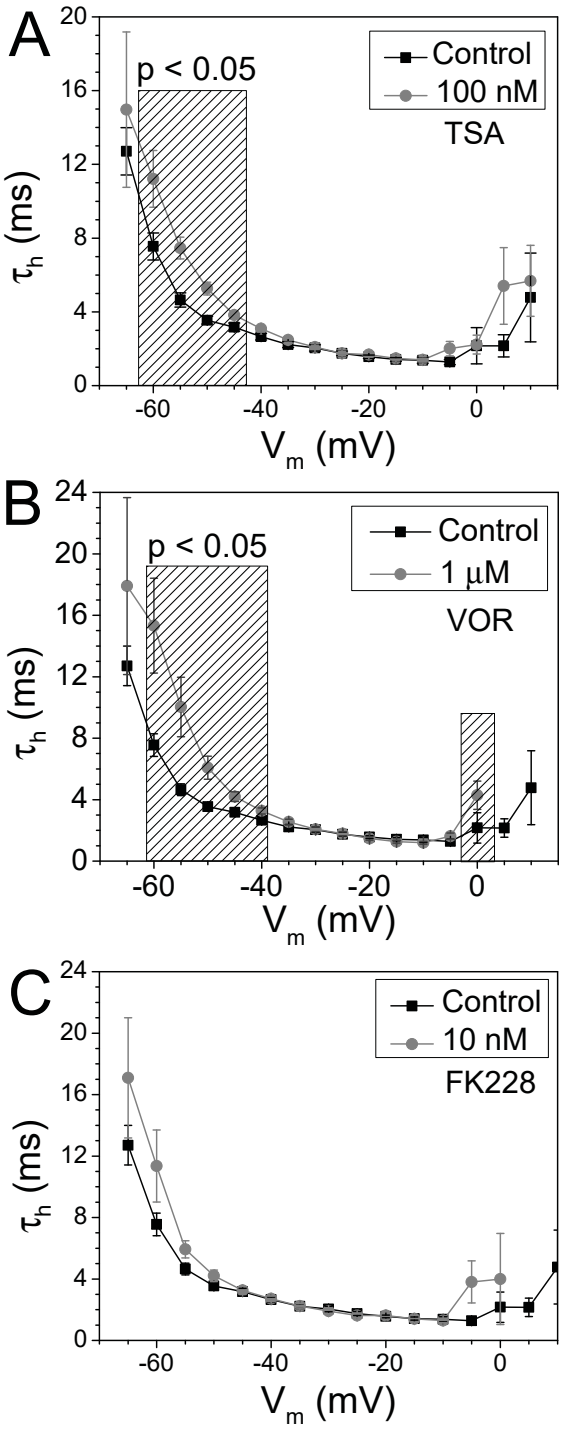
A
p < 0.05
Control
100 nM
TSA
τh (ms)
Vm (mV)
B
p < 0.05
Control
1 μM
VOR
τh (ms)
Vm (mV)
C
Control
10 nM
FK228
τh (ms)
Vm (mV)

Figure 3

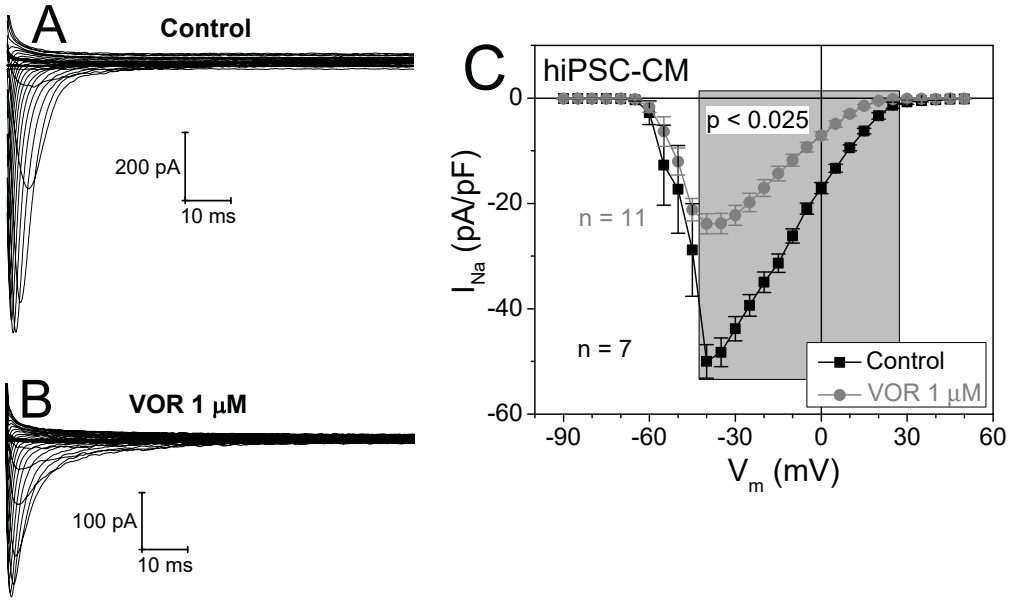
A
Control
200 pA
10 ms
B
VOR 1 μM
100 pA
10 ms
C
hiPSC-CM
p < 0.025
n = 11
n = 7
Control
VOR 1 μM
I_{Na} (pA/pF)
V_m (mV)
0
-20
-40
-60
-90
-60
-30
0
30
60

Figure 4

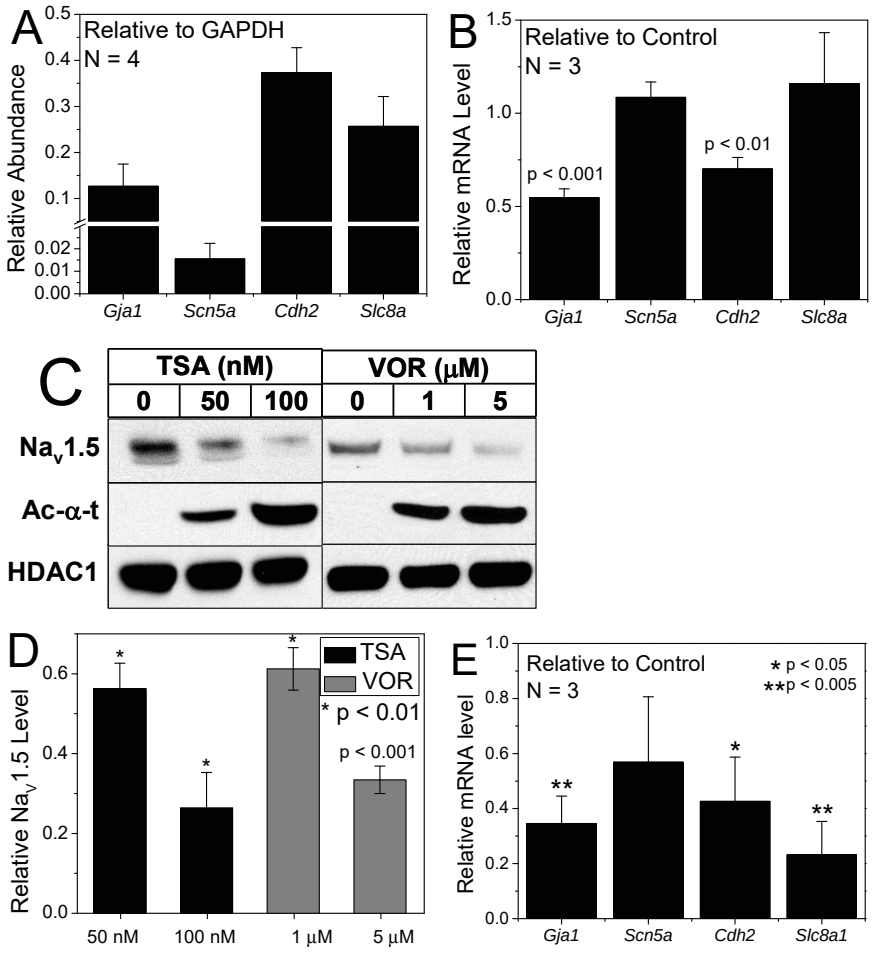
A
Relative to GAPDH
N = 4
Relative Abundance
0.5
0.4
0.3
0.2
0.1
0.02
0.01
0.00
Gja1
Scn5a
Cdh2
Slc8a
B
Relative to Control
N = 3
Relative mRNA Level
1.5
1.0
0.5
0.0
p < 0.001
p < 0.01
Gja1
Scn5a
Cdh2
Slc8a
C
TSA (nM)
VOR (μM)
0
50
100
0
1
5
Nav1.5
Ac-α-t
HDAC1
D
Relative Nav1.5 Level
0.6
0.4
0.2
0.0
TSA
VOR
* p < 0.01
p < 0.001
50 nM
100 nM
1 μM
5 μM
E
Relative to Control
N = 3
* p < 0.05
**p < 0.005
Relative mRNA level
1.0
0.8
0.6
0.4
0.2
0.0
Gja1
Scn5a
Cdh2
Slc8a1

Figure 5

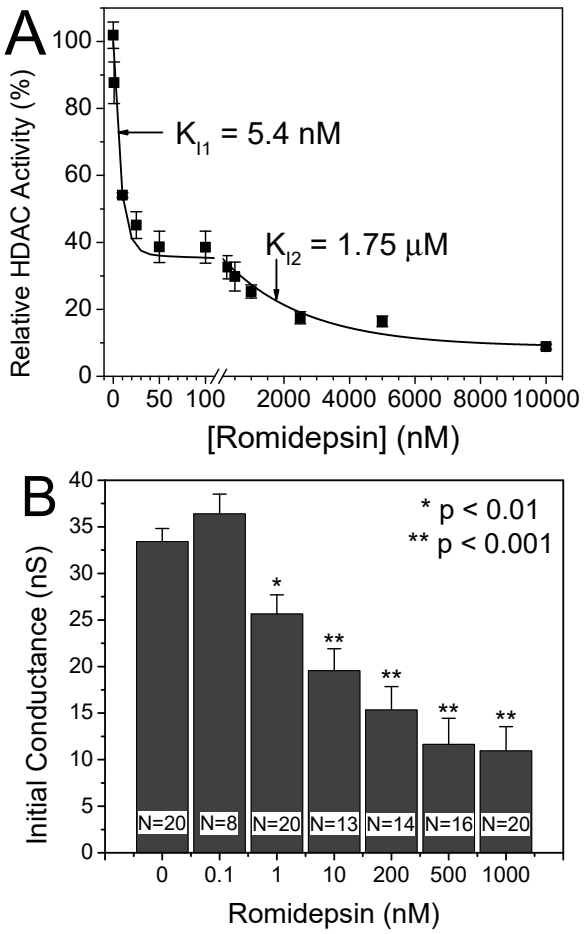
A
Relative HDAC Activity (%)
100
80
60
40
20
0
K_{I1} = 5.4 nM
K_{I2} = 1.75 µM
0 50 100 2000 4000 6000 8000 10000
[Romidepsin] (nM)
B
Initial Conductance (nS)
40
35
30
25
20
15
10
5
0
* p < 0.01
** p < 0.001
*
**
**
**
**
N=20
N=8
N=20
N=13
N=14
N=16
N=20
0 0.1 1 10 200 500 1000
Romidepsin (nM)

Figure 6

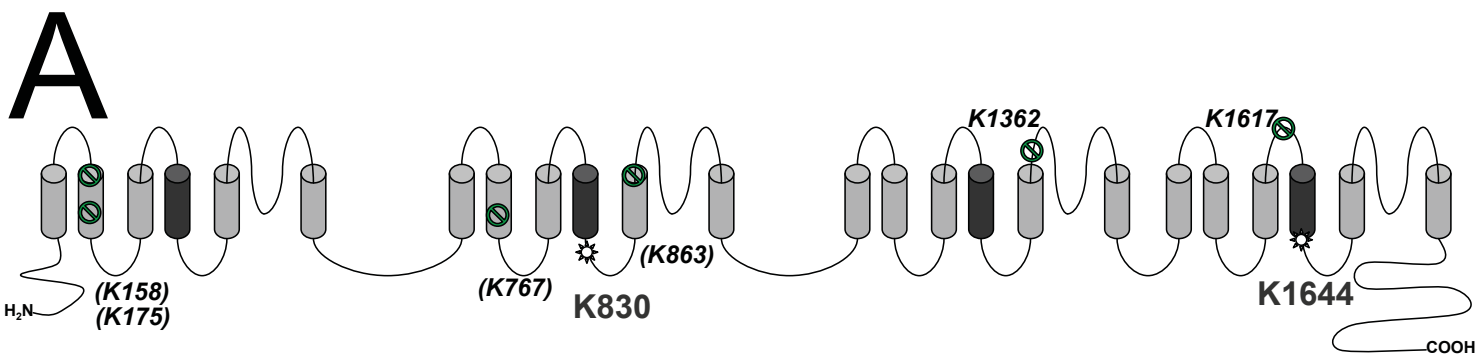
A
K1362
K1617
(K863)
(K158)
(K175)
(K767)
K830
K1644
H2N
COOH

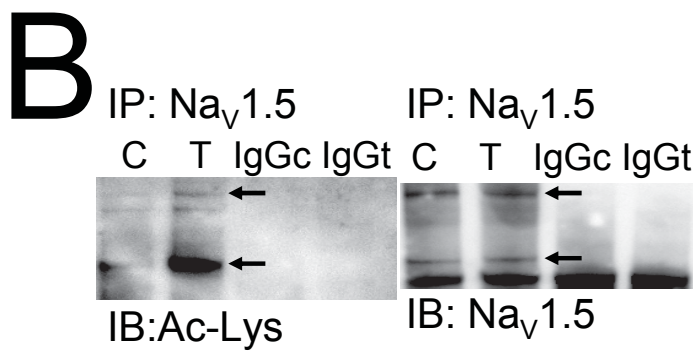
B
IP: NaV1.5
C T IgGc IgGt
IB:Ac-Lys
IP: NaV1.5
C T IgGc IgGt
IB: NaV1.5

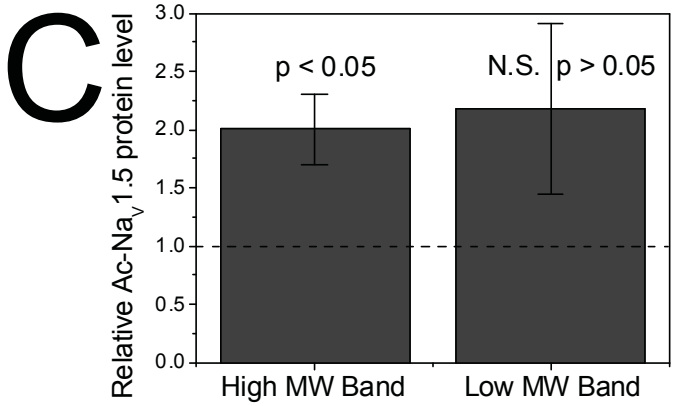
C
Relative Ac-NaV1.5 protein level
3.0
2.5
2.0
1.5
1.0
0.5
0.0
p < 0.05
N.S.
p > 0.05
High MW Band
Low MW Band

Figure 7